Journal Name

COMMUNICATION

"All-in-Gel" Design for Supercapacitors towards Solid-State Energy Devices with Thermal and Mechanical Compliance

Received 00th January 20xx,
Accepted 00th January 20xx

DOI: 10.1039/x0xx00000x

www.rsc.org/

Chengyao Yin,[a] Xinhua Liu,*[b] Junjie Wei,[a] Rui Tan,[d] Jie Zhou,[a] Mengzheng Ouyang,[e] Huizhi Wang,[c] Samuel J. Cooper,[b] Billy Wu,[b] Chandramohan George,[b] and Qigang Wang*[a]

Ionogels are semi-solid, ion conductive and mechanically compliant materials that hold promise for flexible, shape-conformable and all-solid-state energy storage devices. However, identifying facile routes for manufacturing ionogels into devices with highly resilient electrode/electrolyte interfaces remains a challenge. Here we present a novel all-in-gel supercapacitor consisting of an ionogel composite electrolyte and Bucky gel electrodes processed using a one-step method. Compared with the mechanical properties and ionic conductivities of pure ionogels, our composite ionogels offer enhanced self-recovery (retaining 78% of mechanical robustness after 300 cycles at 60% strain) and a high ionic conductivity of 8.7 mS/cm, which is attributed to the robust amorphous polymer phase that enables facile permeation of ionic liquids, facilitating effective diffusion of charge carriers. We show that development of a supercapacitor with these gel electrodes and electrolytes significantly improves the interfacial contact between electrodes and electrolyte, yielding an area specific capacitance of 43 mF/cm² at a current density of 1.0 mA/cm², which represents a 330% improvement compared to Bucky-paper system also investigated. Additionally, through this all-in-gel design a supercapacitor can achieve a capacitance between 22-81 mF/cm² over a wide operating temperature range of -40 to 100 °C at a current density of 0.2 mA/cm².

In order to cope up with the ever evolving market expectations for wearable and portable electronics, energy storage devices need to satisfy increasingly stringent requirements such as being ultra-flexible, lightweight and compact whilst maintaining safety, longevity and endurance under harsh thermal and mechanical abuse.[1–8] This necessitates the development of flexible and shape-conformable electrodes and electrolytes/separators with high mechanical recoverability, with minimal compromise on electrochemical performance.[9–11] Conventional electrochemical energy storage devices typically consist of a separator sandwiched between two electrodes each coated on metallic foil current collectors, all immersed in a liquid electrolyte. Whilst the use of liquid electrolytes typically affords high ionic conductivities and good wettability with the porous electrodes, this can lead to issues such as electrolyte leakage and safety concerns due to the flammability of most organic electrolytes. This limitation can be better mitigated by adopting polymer based all-solid-state energy storage devices that offer new design opportunities in terms of mechanical resilience and longevity, thus making them ideal candidates for developing next-generation wearable electronics.[11–13] However, despite attractive properties including: excellent mechanical robustness, high ionic conductivity and wide operating potential/temperature, barriers to the uptake of polymer based electrolytes still exist which include creating electrode/electrolyte interfaces with electro-mechanical resilience.[14,15]

Recently, several studies relating to flexible all-solid-state energy storage devices have utilized materials such as carbon nanotubes (CNT) or graphene and MXene sheets as flexible electrodes coupled with solid-state polymer gels as electrolytes.[16–21] Also under investigation is the incorporation of carbon materials into ionic liquids (such as Bucky gel) as a route for producing plastic electrodes for actuators.[22–24] Apart from the challenges associated with the fabrication of electrode materials, the design of the electrolyte has become another critical factor, with specific focus on the electrode-electrolyte interfacial compatibility which is key to the device's electro-mechanical performance. Research efforts using polymer based electrolytes have often focused on gelation of aqueous or

[a] School of Chemical Science and Engineering, Tongji University, Shanghai 200092 (P. R. China) E-mail: wangqg66@tongji.edu.cn
[b] Dyson School of Design Engineering, Imperial College London, South Kensington London SW7 2AZ (UK) E-mail: x.liu15@imperial.ac.uk
[c] Department of Mechanical Engineering, Imperial College London, South Kensington London SW7 2AZ (UK)
[d] Department of Chemical Engineering, Imperial College London, South Kensington London SW7 2AZ (UK)
[e] Department of Earth Science and Engineering, Imperial College London, South Kensington London SW7 2AZ (UK)

† Footnotes relating to the title and/or authors should appear here.
Electronic Supplementary Information (ESI) available: [details of any supplementary information available should be included here]. See DOI: 10.1039/x0xx00000x

organic based electrolytes; however, in recent years the use of ionic liquids based gels, known as ionogels, has gained traction. With regards to aqueous based electrolytes, several polymer matrix materials have been investigated and developed to achieve high performance all-solid-state supercapacitors. Meng et al.[25], for instance, reported a highly flexible paper-like polymer supercapacitor with two polyaniline based electrodes infiltrated with and separated by a H_2SO_4-PVA gel electrolyte. However, as the gels mainly consist of a mix of polyvinyl alcohol (PVA) hydrogels or the covalent polymerization of vinyl polymer, they can suffer from brittleness and poor mechanical strength. With regards to utilization of ionogels, Yang et al.[26] developed an all-solid-state supercapacitor which employed commercial activated carbon as an electrode material and an ionically doped-graphene oxide (GO) gel ((PVDF-HFP)-$EMIMBF_4$-GO gel) as an electrolyte. The copolymer acts as a supporting matrix, which contains the ionic liquid electrolyte (1-ethyl-3-methylimidazolium tetrafluoroborate, $EMIMBF_4$), and the GO sheets act as a 3D network which appeared to facilitate ionic transport, resulting in devices with a small internal resistance, high capacitance and good cycle stability.

However, a typical drawback of many gel based supercapacitors is that they can only be operated at near ambient temperatures as their mechanical robustness cannot be maintained above their sol-gel transition temperature, leading to safety concerns when the device is operated at elevated temperatures. For example, the mechanical properties of neutral triblock analogous copolymer and polystyrene–PEO–polystyrene based gel electrolytes quickly degrade when temperature is greater than 60 °C, which may cause short circuit issue.[27] Therefore, it is imperative to develop safe devices by employing thermally and electrochemically stable gel electrolytes matched with suitable gel based electrodes. Moreover, the interfacial contact between the electrodes and the electrolyte strongly depends on the wetting characteristics of electrolytes, and poor design can result in gaps (or inactive regions) at this interface, leading to diminished capacitance.

Keeping the above considerations in mind, we here developed a new "all-in-gel" supercapacitor by employing an ionogel composite electrolyte and ionic liquid based Bucky gel electrode (utilizing the same ionic liquid). Such a design allows for a high ionic conductivity of 8.7 mS/cm, leading to specific capacitance up to 49 mF/cm^2 at 0.1 mA/cm^2. The devices exhibit improved self-healing by retaining 78% of the electrolyte's mechanical robustness even after 300 cycles at 60% strain and are able to operate in a wide temperature range of -40 to 100 °C at a current density of 0.2 mA/cm^2 with reasonable capacitance (22-81 mF/cm^2).

In this work, supercapacitors with symmetrical electrodes were fabricated which consisted of two Bucky gel electrodes separated by

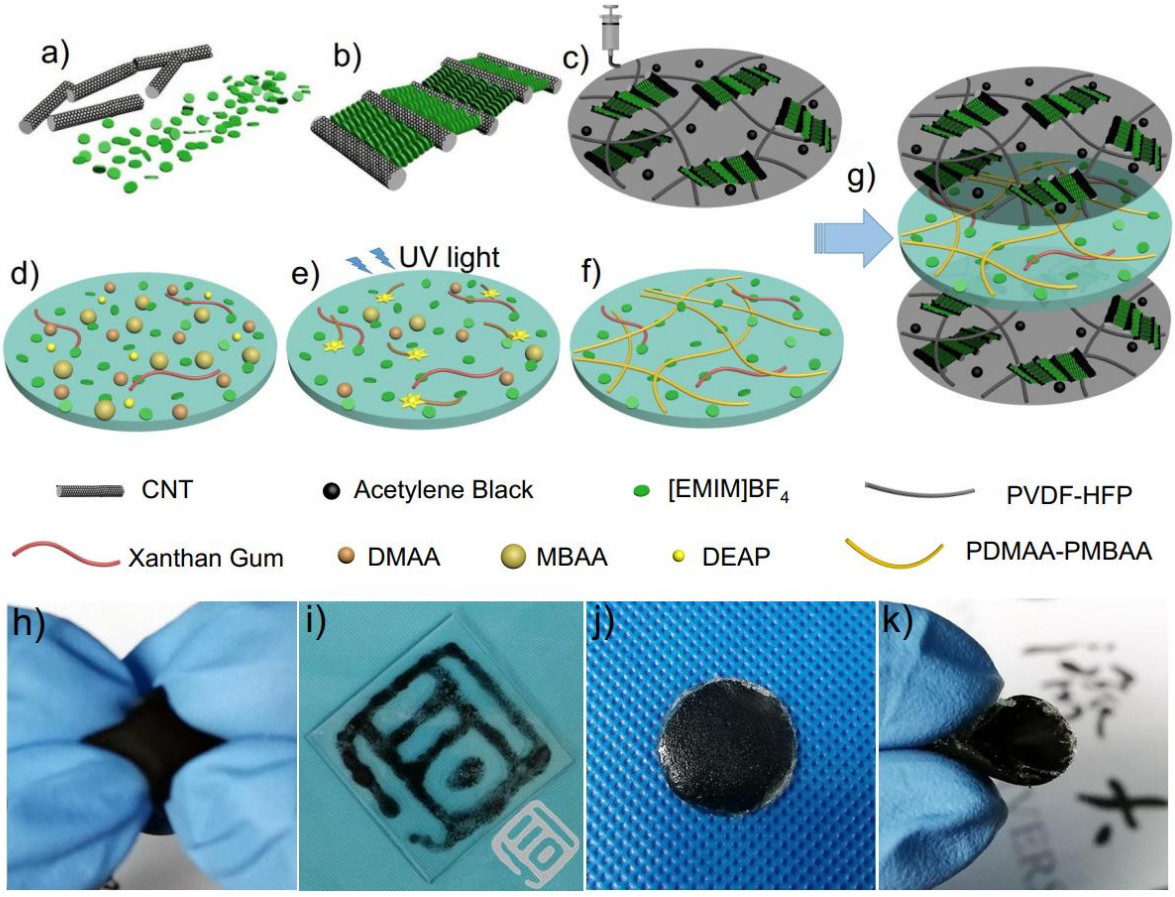

Fig. 1 a) Schematic illustration of carbon nanotube and ionic liquids as main ingredients for these gels, b) after grinding, c) printable Bucky gel electrode. d-f) Schematic diagram of the preparation of Ionogels. g) Schematic illustration of the all-in-gel supercapacitor consisting of a ionogel electrolyte layer sandwiched between two Bucky gel electrodes. Bucky gel electrode can be extruded into various shapes h) Shaping by hand and i) 3D printing (pattern of Tongji logo). j-k) The fabricated all-in-gel supercapacitor in flat and squeezed states.

a composite ionogel electrolyte/separator. The Bucky gel electrodes were prepared by grinding either multi-wall carbon nanotubes (MWCNT), short single-wall carbon nanotubes (SWCNT-s) or long single wall carbon nanotubes (SWCNT-l), 1-ethyl-3-methylimidazolium tetrafluoroborate ($EMIMBF_4$), acetylene black (AB) and poly(vinylidene fluoride-co-hexafluoropropylene) (PVdF-HFP) with a mass ratio of 4:10:1:8 in an agate mortar (Fig. 1a-c)[28–30]. We note that such grinding or mixing in an agate mortar does not appear to change the morphology of the CNTs as shown in the before and after SEM images of Fig. S1. The ionic liquid interacts well with the surface of the SWCNTs by means of cation–π and/or π–π interactions of imidazolium ion component from the ionic liquid.[31,32] The resultant gelatinous materials, the so-called Bucky gel, consisting of conductive carbon nanotubes and fluid electrolytes, are ready-to-use electrodes for supercapacitors and can even be 3D printed. For the ionogel composite electrolyte, the precursor was prepared by mixing the following ingredients as shown in Fig. 1d: xanthan gum (XG), N,N'-Methylenebisacrylamide (MBAA), N,N-dimethylacrylamide (DMAA, 0.5 wt% DEAP) and $EMIMBF_4$ with a mass ratio of 1: 0.15: 20: 80. The resultant precursor was then solidified via UV-irradiation for 20 min to form the ionogel. Herein, the DMAA served as the monomer, MBAA as the cross linker, and DEAP (2,2-Diethoxyacetophenone) as the light-initiator. Upon UV-irradiation, the monomer and the cross linker interact and construct a 3D structure via free radical polymerization (Fig. 1e-f).

After 20 min of UV irradiation, the polymerisation process is more than 99% complete (Fig. S2). The gels can be casted in a variety of shapes which depends on the mold used during the casting and UV-irradiation process. More details on the Bucky gel preparation and device fabrication process can be found in Fig. S3 and the supporting information. Fig. 1g shows the typical all-in-gel design, in which two Bucky gel electrodes are sandwiched either side of an ionogel electrolyte layer (and as separator) to fabricate all-in-gel supercapacitors. Both the Bucky gel and the ionogel contain the same ionic liquid, and because of this, the Bucky gel electrodes can be seamlessly integrated with the ionogel electrolyte such that this all-in-gel device exhibits more intimate and uninterrupted electrode-electrolyte interfacial contact due to the textural compatibility of electrodes. In this regard, the Bucky gel electrode material can be molded into various shapes by hand (Fig. 1h) and can also be 3D printed (pattern of Tongji logo in Fig. 1i). The photographs of the fabricated flexible and shape-conformable all-in-gel supercapacitor are presented in Fig. 1j-k.

As shown in Fig. 2a, the SEM analysis reveals that Bucky gel electrodes have a porous structure consisting of well distributed CNTs, which provide the gel electrodes with high mechanical strength, as well as a percolated pore network providing pathways for facile ion transport. The TEM images of the L-Bucky gel electrode are presented in Fig. S4, which is line with the SEM, confirm the presence of CNTs networks at the nanoscale. Their porous structures were further investigated via N_2 adsorption–desorption isotherms which show that pore size distribution was in the range of 30-60 nm (Fig. S5). Among the different types of carbon nanotubes used for the preparation of the Bucky gels (e.g. multi-wall carbon nanotubes (MWCNT), short single-wall carbon nanotubes (SWCNT-s), and long single wall carbon nanotubes (SWCNT-l), long single-wall carbon nanotubes were identified as optimal for the Bucky gel due to their relatively better electrochemical performance as shown in Fig. S6 and Table S1, which is attributed to the high probability of CNT entanglement, reinforcing the gel electrodes and providing an electronically conducting network. Besides this, the influence of additional conductive agents such as carbon black (CB) and acetylene black (AB) with different mass ratio on the capacitive performance of L-Bucky gel electrodes were studied as shown in Fig. S7 and Table S2, and the electrodes containing SWCNT-AB-10 were found to be the most suitable as they exhibited a capacitance up to 41 mF/cm^2. Therefore, an optimized L-Bucky gel electrode is represented by a mixture of SWCNT-l, $EMIMBF_4$, AB and PVdF-HFP with a mass ratio of 4:10:1:8, as shown in Fig. 2b. For processing the ionogels, XG gum was added to further improve the mechanical strength of the

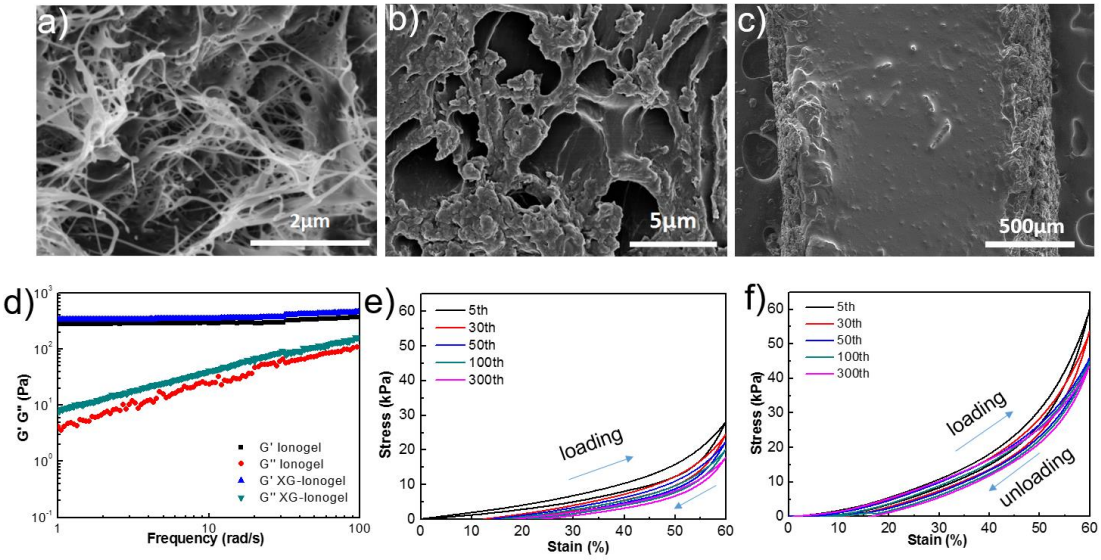

Fig. 2 a) Scanning electron microscopic (SEM) image of the L-Bucky gel electrode. b) SEM image of the XG-ionogel. c) SEM image of the cross section of the all-in-gel supercapacitor. d) Dynamic frequency sweep tests of storage moduli (G') and loss moduli (G'') for the ionogel and XG-ionogel. Compression recovery tests of e) the ionogel and f) the XG-ionogel through 300 cycles with 60% strain.

electrodes because XG gum can promote more crosslinking via hydrogen bonding. Fig. 2d shows that the XG-ionogel has both a higher storage modulus (G') and loss modulus (G''), contributing to improved mechanical performance compared to the pure ionogel (without XG). To understand their gelation kinetics, time sweep measurements were conducted to monitor the evolution of G' and G'' as a function of time (Fig. S8a). At the equilibrium point after approximately 500 s, the value of G' is c. 1.2 times larger than that of the pure ionogel. Fig. S8b also shows the changes of G' and G'' under various strains. Both the frequency sweep tests and the steady rheological behaviours highlight the enhancements made to the mechanical properties of the XG-ionogel versus the pure ionogel. Ionogels with various compositions were also prepared and characterized, and their compressive stress-strain curves are shown in Fig. S9a (various MBAA concentration), Fig. S9c (various DMAA concentration), Fig. S9e (various XG concentration), and their Young's moduli are presented in Fig. S9b, S9d, S9f respectively. The value of Young's modulus increases by roughly a factor of 3 (from 18 kPa to 56 kPa) as the amount of MBAA increases from 0.5 wt% to 1.5 wt% (Fig. S9a and S9b). For other composite variations, the initial values of the Young's moduli follow similar increasing trends. According to Fig. S9c and S9d, the value of Young's modulus increases from 12 kPa to 46 kPa as the amount of DMAA increases from 15 wt% to 25 wt%. Although the addition of XG increases the Young's moduli, the sensitivity between the compressive modulus and the XG concentration appears limited. Therefore, both the Young's modulus and compressive strength were selected as the mechanical indexes for composite optimization. Fig. 2e,f shows the compressive stress-strain curves for the ionogel and XG-ionogel after 300 mechanical cycles at a repeated strain from 0%-60%. The small degree of plastic deformation suggests good elastic behaviour of the XG-ionogels. Furthermore, the XG-ionogel maintains a stress value of 46 kPa even after 300 cycles which is higher than that of the pure ionogel (28 kPa), highlighting the improved mechanical properties and self-recoverability with the addition of XG. FT-IR measurements shown in Fig. S10 compares the spectral features of XG in the XG-ionogel, which is indicative of the preservation of characteristic functional groups of XG in an XG-ionogel mixture, which further accounts for mechanical resilience of the resulting ionogel. The hydrogen bonds between the XG and ionic liquid ($EMIM^+$) can in principle induce effects similar to the ones observed in supramolecular assemblies, giving rise to the formation of 3D polymer networks in XG-ionogels, which can further improve the self-recoverability of these materials after mechanical compression and at the same time this means an optimized amount of XG in ionogels should also be favourable for ionic conductivity. Furthermore, as shown in Fig. S11, the XG-ionogel can easily attach to substrates, for example a carbon cloth, which indicates the strong electrode/electrolyte interface compatibility via the XG-ionogel design. In fact, the SEM image (Fig. 2c) and the enlarged image (Fig. S12) of the cross section of an all-in-gel supercapacitor reveals an intimate interconnection (almost resembling a conformal coating) between the Bucky gel electrode and XG-ionogel. As shown in Fig. S13, compared with the pure Bucky paper electrodes (without the ionic liquid additive), the L-Bucky gel electrodes can achieve better charge/discharge cycling performance, and 3.3 times higher specific capacitance at 1.0 mA/cm². This is attributed to the unique electrode/electrolyte interfaces which are

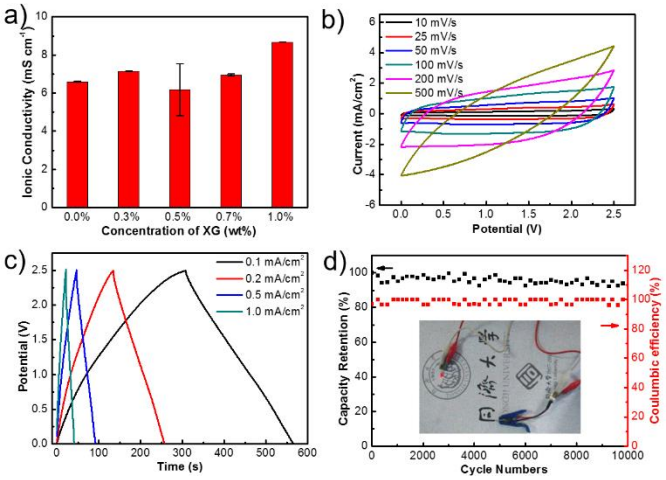

Fig. 3 The electrochemical performance of the all-in-gel supercapacitor (L-Bucky gel electrode) at room temperature. a) The Ionic conductivity values of ionogel applying different XG concentrations. b) Cyclic voltammetry curves with different scan rates. c) Galvanostatic charge-discharge curves with different current density ranging from 0.1 mA/cm² to 1.0 mA/cm². d) Cycling performance of the all-in-gel supercapacitor with 10,000 cycles at a current density of 0.5 mA/cm².

formed through the mixing CNTs with the ionic liquids which induces a high affinity towards each other due to a π-electronic-cation interaction. As opposed to the conventional electrode/electrolyte interfaces (typically between the electronically conductive solid phase and ionically conductive liquid), which tend to present either incompatible interfacial contact due to rigid electrode/electrolyte interface or mechanical issues due to weak interface, the electrodes processed through all-in-gel route contain the electrolyte (ionic liquid) within and across the electrodes and at the electrode/electrolyte interface, giving rise to multiple interfaces, which alleviates both mechanical and interfacial problems across the electrode/electrolyte interface.

Whilst the addition of XG improves the mechanical strength of the XG ionogel, it appears also to improve the ionic conductivity. Fig. 3a presents the ionic conductivities of the XG-ionogel with various XG concentrations. A high ionic conductivity of 8.7 mS/cm is achieved for the XG-ionogel with 1 wt% XG. This is probably due to the presence of more charge carriers with 1% XG and also due to the ability of XG in acting as a structural promotor (i.e XG and ionic liquid ($EMIM^+$) triggering supramolecular like assemblies more conducive to ionic conductivities. After preparing the gels with optimized electronic (CNT length, carbon additive), ionic (ionic liquid, XG), mechanical (CNTs and XG) and electrochemical properties of the gels with different composition, the XG-ionogels with a composition 1.0 wt% XG and 20 wt% DMAA (0.15 wt% MBAA) was used as both electrolyte and separator in the all-in-gel supercapacitor. Fig. 3b shows the cyclic voltammograms of the all-in-gel supercapacitor at room temperature, showing a good capacitive performance at various scan rates. The calculated specific capacitance was 41 mF/cm² at 10 mV/s, which drops to 33 mF/cm² at 100 mV/s. As shown in Fig. 3c, the charge/discharge curves are relatively linear and symmetric at different current densities from 0.1-1.0 mA/cm², pointing to good electrochemical reversibility. The specific capacitance was then calculated to be 49 mF/cm² (62 F/g) at 0.1

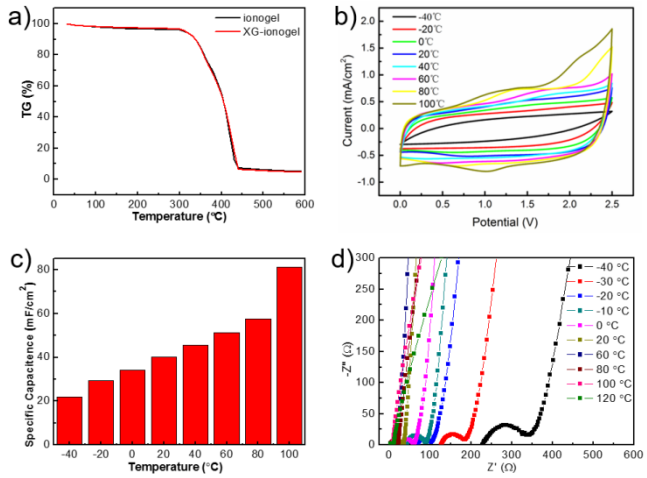

Fig. 4 a) The thermo gravimetric analysis of ionogel and XG-ionogel. a) The temperature dependent cyclic voltammetry curves of the all-in-gel supercapacitor (L-Bucky gel electrode) at a scan rate of 50 mV/s. c) The area specific capacitance at 0.2 mA/cm^2 current density applying different temperatures ranging from -40 °C to 100 °C. d) Nyquist plots applying different temperatures (from -40 to 100 °C).

mA/cm^2 and maintained at 43 mF/cm^2 (54 F/g) at 1.0 mA/cm^2 (Fig. S14 and Table S3), with current densities demonstrated as high as 10 mA/cm^2 (Fig. S15). Fig. 3d shows the excellent cycling performance of the all-in-gel supercapacitor at 0.5 mA/cm^2 over 10,000 cycles which is attributed to the electrochemical stability of the ionic liquid. After cycling tests, the interface between Bucky gel electrode and ionogel electrolyte was analysed via SEM (See Fig S16). No significant or noticeable changes could be observed, which is indicative of a better interfacial compatibility due to matched electrodes and electrolyte in terms of structural compatibility, proving the stability of the all-in-gel configuration. Table S4 in the supporting information compares the performance of our electrodes with some of the similar electrodes recently reported. The high thermal stability of the composite ionogel is shown by thermal gravimetric analysis (TGA) results in Fig. 4a, which shows a very low mass loss up to ca. 300 °C, after which the material degrades rapidly. As shown in Fig. 4b, the shape of the cyclic voltammetry (CV) curves tested at 50 mV/s becomes increasingly rectangular as the temperature increases from -40 °C to 100 °C. The specific capacitance of the device measured at 0.2 mA/cm^2 indicates a strong temperature dependence (Fig. 4c), with a monotonic increase from 22 to 81 mF/cm^2 when the temperature increases from -40 °C to 100 °C. This is likely due to the increased ionic conductivity, which reaches a maximum value of 15.3 mS/cm at 100 °C and follows an Arrhenius type trend (Fig. S17). The ionic liquid has a wide temperature range in which it retains the liquid state, whilst the polymer matrix itself can provide ion transfer pathways, therefore, even at the low temperature of -40 °C, the ionogel device can still maintain a reasonable capacitive performance. The ionic conductivity of the polymer matrix can be attributed to the amorphous domains[33,34],leading to an improved performance compared to a conventional insulating separator[35,36]. Fig. 4d shows electrochemical impedance spectroscopy (EIS) data collected at a range of temperatures. There is a clear trend towards lower impedance as temperature increases, which is most likely due to the result of improved ionic conductivities as previously discussed. However, in addition to a reduction in the high frequency real axis intercept (typically associated with the ionic transport between the two electrodes), there is also a reduction in the width of a semicircle feature at intermediate frequencies. These semicircle features are often attributed to a variety of pseudo-capacitive processes taking place in the supercapacitor, which is in line with previous reports[37] but can also be more simply explained by considering a spatially distributed nature of capacitive surface in porous electrodes as reported by Eloot et al.[38]

Conclusions

In conclusion, we presented a novel all-in-gel design for all-solid-state energy storage devices by employing ionogel composite electrolytes and Bucky gel electrodes that possess enhanced mechanical strength and ionic conductivity. These ionogel composites can act both as integrated electrolyte and separator, which overcomes the typical interfacial and mechanical issues across electrode/electrolyte interfaces (as in conventional designs) by facilitating an intimate and mechanically resilient contact. As a result, all-solid-state supercapacitors fabricated through the seamless integration of an $EMIMBF_4$-based ionogel electrolyte/separator with $EMIMBF_4$-based Bucky electrodes not only offer ionic conductivities up to 8.7 mS/cm, resulting in high capacitance of 41 mF/cm^2 at 10 mV/s but allow for a wide operating temperature range of (-40 to 100 °C) with capacitance of 22-81 mF/cm^2. These ionogel electrolytes are stable up to 300° C and 78% self-recoverable under a high strain of 60%. These soft, flexible, shape-conformable and easy-to-manufacture all-in-gel materials represent a step change in the design of safe energy storage devices for wearable electronics, in particular those facing the increased demands of hazardous operational environments.

Conflicts of interest

There are no conflicts to declare.

Acknowledgment

This work was kindly supported by the National Natural Science Foundation of China (No. 51473123) of QW; the EPSRC energy storage for low carbon grids project (EP/K002252/1), the EPSRC Joint UK-India Clean Energy center (JUICE)(EP/P003605/1), the Integrated Development of Low-Carbon Energy Systems (IDLES) project (EP/R045518/1), the Innovate UK BAFTA project, and the Innovate UK for Advanced Battery Lifetime Extension (ABLE) project of XL and BW; the EPSRC for funding under EP/S000933/1 of HW and The Royal Society of London for an URF of CG.

Notes and references

1 X. Liu, Z. Wen, D. Wu, H. Wang, J. Yang and Q. Wang, *J. Mater. Chem. A*, 2014, **2**, 11569–11573.

2 S. E. Root, S. Savagatrup, A. D. Printz, D. Rodriquez and D. J. Lipomi, *Chem. Rev.*, 2017, **117**, 6467–6499.

3 M. G. Mohammed and R. Kramer, *Adv. Mater.*, 2017, **29**, 1604965.

4 J. Deng, X. Kuang, R. Liu, W. Ding, A. C. Wang, Y. C. Lai, K. Dong, Z. Wen, Y. Wang, L. Wang, H. J. Qi, T. Zhang and Z. L. Wang, *Adv. Mater.*, 2018, **30**, 1–10.

5 Y. Yang and W. Gao, *Chem. Soc. Rev.*, 2019, **48**, 1465-1491.

6 D. P. Dubal, N. R. Chodankar, D. H. Kim and P. Gomez-Romero, *Chem. Soc. Rev.*, 2018, **47**, 2065–2129.

7 D. Wang, Y. Zhang, X. Lu, Z. Ma, C. Xie and Z. Zheng, *Chem. Soc. Rev.*, 2018, **47**, 4611–4641.

8 Y. Liu, M. Pharr and G. A. Salvatore, *ACS Nano*, 2017, **11**, 9614–9635.

9 Z. Niu, W. Zhou, X. Chen, J. Chen and S. Xie, *Adv. Mater.*, 2015, **27**, 6002–6008.

10 X. Liu, B. Wu, N. Brandon and Q. Wang, *Energy Technol.*, 2017, **5**, 220-224.

11 X. Liu, D. Wu, H. Wang and Q. Wang, *Adv. Mater.*, 2014, **26**, 4370-4375.

12 Q. Liao, N. Li, S. Jin, G. Yang and C. Wang, *ACS Nano*, 2015, **9**, 5310–5317.

13 Y. Y. Peng, B. Akuzum, N. Kurra, M. Q. Zhao, M. Alhabeb, B. Anasori, E. C. Kumbur, H. N. Alshareef, M. Der Ger and Y. Gogotsi, *Energy Environ. Sci.*, 2016, **9**, 2847–2854.

14 D. Qi, Y. Liu, Z. Liu, L. Zhang and X. Chen, *Adv. Mater.*, 2017, **29**, 1–19.

15 L. Li, Z. Wu, S. Yuan and X. B. Zhang, *Energy Environ. Sci.*, 2014, **7**, 2101–2122.

16 Y. Ma, P. Li, J. W. Sedloff, X. Zhang, H. Zhang and J. Liu, *ACS Nano*, 2015, **9**, 1352–1359.

17 Z. Zhang, F. Xiao, L. Qian, J. Xiao, S. Wang and Y. Liu, *Adv. Energy Mater.*, 2014, **4**, 1–9.

18 Z. Pan, M. Liu, J. Yang, Y. Qiu, W. Li, Y. Xu, X. Zhang and Y. Zhang, *Adv. Funct. Mater.*, 2017, **27**, 1–9.

19 L. Wen, F. Li and H. M. Cheng, *Adv. Mater.*, 2016, **28**, 4306–4337.

20 M. Q. Zhao, C. E. Ren, Z. Ling, M. R. Lukatskaya, C. Zhang, K. L. Van Aken, M. W. Barsoum and Y. Gogotsi, *Adv. Mater.*, 2015, **27**, 339–345.

21 B. Deng, P. C. Hsu, G. Chen, B. N. Chandrashekar, L. Liao, Z. Ayitimuda, J. Wu, Y. Guo, L. Lin, Y. Zhou, M. Aisijiang, Q. Xie, Y. Cui, Z. Liu and H. Peng, *Nano Lett.*, 2015, **15**, 4206–4213.

22 T. Fukushima, A. Kosaka, Y. Ishimura, T. Yamamoto, T. Takigawa, N. Ishii and T. Aida, *Science (80-.).*, 2003, **300**, 2072–2074.

23 I. Katayama, Z. Jiang, T. Hiraga, S. Karato, K. M. Fischer, J. F. Cassidy, R. D. Hyndman, M. G. Bostock, R. D. Van Der Hilst, D. A. Wiens, J. A. Conder, H. Shiobara, H. Sugioka, K. M. Fischer, E. M. Parmentier, D. K. Blackman, G. Hirth, P. B. Keleman, P. G. Silver, B. R. Hacker, G. Hirth, P. G. Kelemen, A. Hasegawa, P. E. Van Keken, J. Park, B. H. Hager, M. V. De Hoop, R. D. Van Der Hilst, S. Lallemand, G. A. Abers, R. D. Van Der Hilst, D. Droznin, J. Park, E. Gordeev, N. M. Ribe, R. W. Griffiths, P. E. Van Keken, J. Hasenclever, M. Hort, E. M. Parmentier, C. Faccenna, C. P. Conrad and A. Tsunami, 2008, 318–321.

24 T. Fukushima, K. Asaka, A. Kosaka and T. Aida, *Angew. Chemie - Int. Ed.*, 2005, **44**, 2410–2413.

25 C. Meng, C. Liu, L. Chen, C. Hu and S. Fan, *Nano Lett.*, 2010, **10**, 4025–4031.

26 X. Yang, F. Zhang, L. Zhang, T. Zhang, Y. Huang and Y. Chen, *Adv. Funct. Mater.*, 2013, **23**, 3353–3360.

27 X. Lin, M. Salari, LMR. Arava, PM. Ajayan, MW. Grinstaff, *Chem. Soc. Rev.*, 2016, **45**, 5848-5887.

28 R. Boldt, M. Mende, G. Petzold, T. Villmow, P. Pötschke and B. Krause, *Compos. Sci. Technol.*, 2011, **71**, 1145–1153.

29 B. Munkhbayar, M. J. Nine, S. Hwang, J. Kim, K. Bae, H. Chung and H. Jeong, *Chem. Eng. Process. Process Intensif.*, 2012, **61**, 36–41.

30 M. Zhu, H. Xiang, S. Yu, L. Zhu, X. Wang and M. Tebyetekerwa, *Carbon N. Y.*, 2018, **140**, 1–9.

31 T. Fukushima, A. Kosaka, Y. Ishimura, T. Yamamoto, T. Takigawa, N. Ishii and T. Aida, 2003, **300**, 2072–2075.

32 T. Fukushima and T. Aida, 2007, 5048–5058.

33 X. Zhang, M. Kar, T. C. Mendes, Y. Wu and D. R. Macfarlane, *Adv. Energy Mater.*, 2018, **1702702**, 1–8.

34 M. Jin, Y. Zhang, C. Yan, Y. Fu, Y. Guo and X. Ma, *ACS Appl. Mater. Interfaces*, 2018, **10**, 39570–39580.

35 A. Chandra, 2012, **82**, 79–90.

36 P. Sharma and T. S. Bhatti, *Energy Convers. Manag.*, 2010, **51**, 2901–2912.

37 X. Liu, O. O. Taiwo, C. Yin, M. Ouyang, R. Chowdhury, B. Wang, H. Wang, B. Wu, N. P. Brandon, Q. Wang and S. J. Cooper, *Adv. Sci.*, 2018, **1801337**, 1–7.

38 K. Eloot, F. Debuyck, M. Moors and A. P. Van Peteghem, *J. Appl. Electrochem.*, 1995, **25**, 326–333.